



**HAL**  
open science

# Interactions between nanoscale zerovalent iron (NZVI) and silver nanoparticles alter the NZVI reactivity in aqueous environments

J. Deng, S. Yoon, M. Pasturel, S. Bae, Khalil Hanna

## ► To cite this version:

J. Deng, S. Yoon, M. Pasturel, S. Bae, Khalil Hanna. Interactions between nanoscale zerovalent iron (NZVI) and silver nanoparticles alter the NZVI reactivity in aqueous environments. *Chemical Engineering Journal*, 2022, 450, pp.138406. 10.1016/j.cej.2022.138406 . hal-03780242

**HAL Id: hal-03780242**

**<https://hal.science/hal-03780242v1>**

Submitted on 9 Feb 2023

**HAL** is a multi-disciplinary open access archive for the deposit and dissemination of scientific research documents, whether they are published or not. The documents may come from teaching and research institutions in France or abroad, or from public or private research centers.

L'archive ouverte pluridisciplinaire **HAL**, est destinée au dépôt et à la diffusion de documents scientifiques de niveau recherche, publiés ou non, émanant des établissements d'enseignement et de recherche français ou étrangers, des laboratoires publics ou privés.

1

2 **Interactions between nanoscale zerovalent**  
3 **iron (NZVI) and silver nanoparticles alter**  
4 **the NZVI reactivity in aqueous**  
5 **environments**

6

7 Junmin Deng<sup>1</sup>, Sunho Yoon<sup>2</sup>, Mathieu Pasturel<sup>3</sup>, Sungjun Bae<sup>2\*</sup>, Khalil Hanna<sup>1\*</sup>

8

9 <sup>1</sup> *Univ. Rennes, Ecole Nationale Supérieure de Chimie de Rennes, CNRS, ISCR-UMR*

10 *6226, F-35000 Rennes, France*

11 <sup>2</sup> *Department of Civil and Environmental Engineering, Konkuk University, 120*

12 *Neungdong-ro, Gwangjin-gu, Seoul 05029, Republic of Korea*

13 <sup>3</sup> *Univ. Rennes, CNRS, ISCR – UMR 6226, F-35000 Rennes, France*

14

15 \*Co-corresponding authors: [khalil.hanna@ensc-rennes.fr](mailto:khalil.hanna@ensc-rennes.fr) and [bsj1003@konkuk.ac.kr](mailto:bsj1003@konkuk.ac.kr)

16

17

18 **ABSTRACT**

19 The increasing production and broad application of engineered nanoparticles  
20 (ENPs) have led to a substantial release of ENPs into natural systems. Despite their  
21 different utilization prospects, ENPs such as nanoscale zero-valent iron (NZVI) and  
22 silver nanoparticles (AgNPs) have been co-found in aquatic environments. This study  
23 comprehensively examined the effect of AgNPs on the reductive ability of NZVI, which  
24 was probed through the conversion of *p*-nitrophenol (*p*-NP) to *p*-aminophenol (*p*-AP).  
25 Electron microscopic and spectroscopic investigations and Derjaguin–Landau–  
26 Verwey–Overbeek (DLVO) calculations showed that the aggregation of NZVI with a  
27 low dose of AgNPs dramatically decreased the NZVI reactivity. In contrast, enhanced  
28 NZVI reactivity was observed when a high dose of AgNPs was used. The collision  
29 between self-assembled aggregates of AgNPs and NZVI can lead to the exposure of  
30 inner Fe(0), thereby improving the reductive ability of NZVI. The same behavior was  
31 observed for other nanosized (e.g., TiO<sub>2</sub>) and microsized (e.g., quartz sand) particles,  
32 which suggests the predominance of physical processes in NZVI peeling. Further  
33 investigations showed that the presence of sulfate and humic acid enhanced the *p*-NP  
34 removal in the NZVI-AgNP suspension, in contrast to other groundwater constituents.  
35 Our findings provide a better understanding of potential ENP interactions, particularly  
36 in the context of groundwater remediation.

37 **Keywords:** nanoscale zerovalent iron; silver nanoparticles; *p*-nitrophenol; aggregation.

38

39

### Graphical Abstract

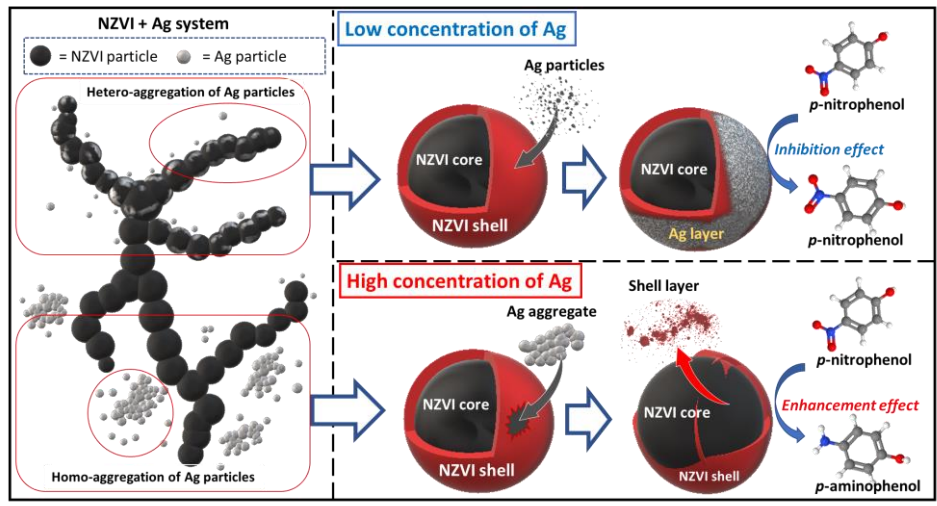
40

Interactions between nanoscale zero-valent iron (NZVI) and silver nanoparticles

41

(AgNPs) significantly alter the reductive ability of NZVI

42



43

44

## 45 **1. Introduction**

46 Over the past decades, due to increasing production and broad applications of  
47 engineered nanoparticles (ENPs), such as textile (Lorenz et al., 2012), electronics  
48 (Poudel and Kim, 2022; Poudel et al., 2021), pharmaceuticals (Sridhar et al., 2015),  
49 environmental remediation (Poudel et al. 2022) and cosmetics (Auffan et al., 2010), a  
50 significant amount of ENPs are ended up into natural systems (Abbas et al., 2020;  
51 Danaïl and Ineke, 2009). In particular, silver nanoparticles (AgNPs) are one of the most  
52 commonly used ENPs. Their catalytic ability, high surface area to volume ratio and  
53 antibacterial activity provide them with excellent potential for various industrial  
54 (Poudel et al., 2020; Shen et al., 2014), food (Echegoyen and Nerín, 2013) and medical  
55 applications (Deng et al., 2016). However, their release and accumulation in the  
56 environment (water and soil) (McGillicuddy et al., 2018; Mahdi et al., 2017) is of  
57 concern owing to their potential adverse effects on human health and aquatic life  
58 (Asghari et al., 2012; Xu et al., 2013). In the meanwhile, nanoscale zero-valent iron  
59 (NZVI), as one of the most extensively used ENPs, has been widely applied for  
60 groundwater remediation and wastewater treatment because of its high reactivity, cost-  
61 effectiveness, and environmental friendliness (Li et al., 2017; Phenrat et al., 2016; Wei  
62 et al., 2010; Xia et al., 2017). NZVI can be used to treat various contaminants such as  
63 persistent organic pollutants (Joo et al., 2004), toxic inorganic contaminants (Ryu et al.,  
64 2011) and even radioactive nuclides (Tsarev et al., 2017).

65 When AgNPs are discharged into terrestrial or aquatic environments, their

66 interaction with other co-existing ENPs could influence their environmental behavior,  
67 fate, and likely their ecotoxicity. In addition, AgNPs can potentially alter the reactivity  
68 of other ENPs used for decontamination, such as NZVI. The injection of NZVI slurry  
69 is a common method for the *in situ* remediations of aquifer and groundwater  
70 contamination by organic or inorganic compounds (Su et al., 2013; Mueller et al., 2012).  
71 Despite the possible co-occurrence of both ENPs in aquatic environments (Stefaniuk et  
72 al., 2016; Syafiuddin et al., 2018), there is a lack of knowledge on their potential  
73 interactions. Therefore, a comprehensive study on the interactions between NZVI and  
74 AgNPs is needed considering the contaminant removal methods used in remediation  
75 processes.

76 Herein, we selected *p*-nitrophenol (*p*-NP), as a probe compound because the  
77 reductive conversion of *p*-NP to *p*-aminophenol (*p*-AP) is well documented, and the  
78 corresponding mass balance is easy to establish owing to the low adsorption of  
79 nitrophenol and aminophenol by metal oxides (Bae et al., 2016; Lai et al., 2014; Vilardi  
80 2020). In order to investigate the interactions between NZVI and AgNPs and clearly  
81 highlight specific effects of AgNPs on the NZVI reductive ability, we applied a wide  
82 concentration range and high-enough dosage of AgNPs (0.5 – 100 mg/L) in NZVI  
83 suspension. Two concentrations of NZVI (25 and 50 mg/L) within the concentration  
84 range typically used in lab-experiments were investigated. The phase transformation  
85 and morphological change of NZVI and AgNPs were monitored by X-ray diffraction  
86 (XRD), X-ray photoelectron spectroscopy (XPS), and transmission electron

87 microscopy (TEM) with energy-dispersive X-ray spectroscopy (EDS). In addition, a  
88 theoretical investigation based on Derjaguin–Landau–Verwey–Overbeek (DLVO)  
89 calculations were conducted for the low and high doses of AgNPs. Moreover, to get  
90 more insight into the relationship between effects of ENPs and their nature, interactions  
91 of NZVI with other widely used ENPs (e.g. nanosized TiO<sub>2</sub> particles) and inert mineral  
92 surface (e.g. quartz sand) were also investigated. Finally, the NZVI-AgNP interactions  
93 were evaluated in the presence of naturally occurring anions and cations and natural  
94 organic matter, at levels similar to those encountered in real groundwater.

95

## 96 **2. Materials and methods**

### 97 *2.1 Chemicals and materials*

98 Sodium borohydride (NaBH<sub>4</sub>, ≥99.0%), *p*-NP (≥99%), *p*-AP (≥98%), ferric  
99 chloride hexahydrate (FeCl<sub>3</sub>·6H<sub>2</sub>O, ≥99.0%), hydrochloric acid (HCl, 37%), sodium  
100 hydroxide (NaOH, ≥99.0%), sodium chloride (NaCl, ≥99.5%), sodium sulfate (Na<sub>2</sub>SO<sub>4</sub>,  
101 ≥99.0%), calcium chloride (CaCl<sub>2</sub>, ≥99.9%), magnesium chloride (MgCl<sub>2</sub>, ≥98.0%) and  
102 sodium metasilicate nonahydrate (Na<sub>2</sub>SiO<sub>3</sub>·9H<sub>2</sub>O, ≥98.0%) were purchased from  
103 Sigma-Aldrich, France. Acetonitrile (99.99%, Sigma) and acetic acid (99.7%, ACROS)  
104 were used as the mobile phase for the high-performance liquid chromatography (HPLC)  
105 analysis. Leonardite humic acid (LHA) standard was purchased from the International  
106 Humic Substances Society (IHSS). Silver nano-powder (containing  
107 polyvinylpyrrolidone (PVP) as a dispersant, 99.5%, <100 nm, and PZC ~3.3) and TiO<sub>2</sub>

108 nano-powder (rutile, 99.5%, 50 m<sup>2</sup>/g, <100 nm, and PZC ~5.9) were purchased from  
109 Sigma-Aldrich. Fontainebleau quartz sand (FB sand, 0.06 m<sup>2</sup>/g, 150–300 μm, PZC ~2.7)  
110 was obtained from VWR International. Based on a previously published method (Deng  
111 et al., 2020), NZVI was synthesized by reducing 0.11 M FeCl<sub>3</sub>·6H<sub>2</sub>O with 0.9 M NaBH<sub>4</sub>  
112 in an anaerobic chamber.

113 The glassware was soaked in 5% (v:v) HCl for at least 48 h and rinsed before use.  
114 Unless specifically stated, all solutions were prepared with deoxygenated deionized  
115 water (DDIW, 18.2 MΩ·cm), purged with nitrogen (N<sub>2</sub>, 99.99%) for 4 h, and stored in  
116 an anaerobic chamber (JACOMEX).

117

## 118 *2.2. Experimental and analytical methods*

119 Batch experiments were conducted in 500 mL flask in an anaerobic chamber under  
120 dark conditions. An exact amount of NZVI (0.0125 and 0.025 g) was transferred to the  
121 flask containing 500 mL of DDIW, and the mixture was stirred at 500 rpm to prepare  
122 the samples with initial NZVI concentrations of 25 and 50 mg/L. To monitor the  
123 variations in pH and oxidation-reduction potential (ORP) throughout the experiment,  
124 we used a portable pH–ORP meter (HI991003, Hanna). After 1 h, AgNPs were  
125 introduced into the suspensions to form a mixture of NZVI and AgNPs at different Ag  
126 concentrations (0.5, 2, 10, 25, 50, and 100 mg/L). An equilibration time of 1 hour was  
127 chosen because pH and ORP values have reached constant values after 1 h of reaction time.  
128 Although this time is sufficient to obtain an equilibrated NZVI suspension under our



129 experimental conditions, it may not be applicable at the field-scale.

130 After 15 h, pH and ORP reached an equilibrium, and 2 mL of *p*-NP stock solution  
131 (25 mM) was added to the suspension to initiate the reaction with *p*-NP (0.1 mM).  
132 Subsequently, 1 mL samples were withdrawn from the suspension and then filtered  
133 through a 0.2  $\mu$ m filter (Whatman) for HPLC analysis. The aqueous concentrations of  
134 *p*-NP and *p*-AP were determined using HPLC (Waters 600 controller) with a photodiode  
135 array detector (Waters 996) and a reversed-phase C18 column (250 mm  $\times$  4.6 mm i.d.,  
136 5  $\mu$ m). A mobile phase (acetonitrile: water at 50:50 (v:v)) containing 0.1% formic acid  
137 was prepared and used at a flow rate of 1 mL/min in isocratic mode. In addition, mass  
138 balance of *p*-NP and *p*-AP after reaction was checked and presented in Table S1.

139 The same procedure was used to investigate the effects of TiO<sub>2</sub> nanoparticles, FB  
140 sand, and groundwater solutes on the reactivity of NZVI and NZVI/AgNPs. The AgNP  
141 dissolution experiments were conducted at pH 9 in absence of NZVI, which is similar  
142 to the working pH in presence of NZVI, at AgNP dosage of 0.5, 2, 10, 25, 50, and 100  
143 mg/L. Although the dosage of AgNPs seems to be higher than the frequently detected  
144 concentration in natural systems, we have assessed the interactions of NZVI with  
145 AgNPs over a wide range of Fe/Ag ratios (0.5 - 50) to cover some environmentally-  
146 relevant scenarios.

147 After 3 d, the samples were filtered through a 0.2  $\mu$ m filter to measure the amount  
148 of Ag<sup>+</sup> ions by inductively coupled plasma mass spectrometry (ICP-MS, Agilent 7700x).  
149 All experiments were performed in triplicates. The data reported here are the average

150 of three replicated experiments, and the error bars represent the relative standard  
151 deviation.

152

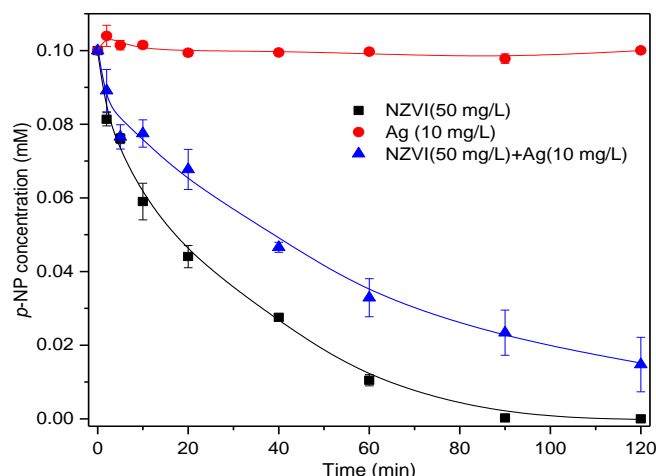
### 153 *2.3. Characterization*

154 XRD (D8, BRUKER) was used to identify the resulting products of NZVI after  
155 reaction with *p*-NP. The resulting suspensions were first collected and washed with  
156 DDIW three times, and dried in a vacuum freeze drier (−52 °C, 24 h). The dried samples  
157 were then transferred to sample holders and treated with 1:1 (v:v) glycerol solution to  
158 avoid surface oxidation during the XRD analysis (Bae and Lee, 2014). XPS (Sigma  
159 Probe system, Thermo) analysis was performed for NZVI, AgNPs, and NZVI-AgNP  
160 samples. The power source (Al K $\alpha$  X-ray, 1486.7 eV) was 75 W, and the C 1s peak at  
161 285 eV was used as a reference for the correction of surface charging effects. The  
162 morphological characterization of the NZVI and NZVI-AgNP mixtures was performed  
163 by TEM–EDS, (JEM-2100, JEOL). The average particle size of the NZVI-AgNP  
164 suspension with groundwater solutes and the zeta potential of individual particles (i.e.,  
165 NZVI and AgNPs) were measured using a Zetasizer (Matec Applied Sciences). The  
166 average hydrodynamic diameter of AgNPs and NZVI were determined using time-  
167 resolved dynamic light scattering (DLS, ALV-5000, Langen).

168

## 169 **3. Results and discussion**

### 170 *3.1 Effect of AgNPs on the NZVI reactivity*



171

172 Figure 1. Concentrations of *p*-NP during the removal of *p*-NP by different nanoparticles.

173 Experimental conditions: [*p*-NP]<sub>initial</sub> = 0.1 mM; [NZVI] = 50 mg/L; [AgNPs] = 10  
 174 mg/L; pH = 9.0±0.2.

175

176 The interactions between AgNPs and NZVI were investigated under anoxic  
 177 conditions by monitoring the variations in pH and ORP throughout the experiment,  
 178 including at i) the addition of NZVI to the reactor, ii) addition of AgNPs, and iii)  
 179 removal of *p*-NP (see Supporting Information (SI), Fig. S1). When NZVI was added to  
 180 water at 50 mg/L (i.e., first 1 h), there was a clear increase in pH from 6.78 to 9.38 and  
 181 a decrease in ORP from -54 to -843 mV, which were attributed to the reaction between  
 182 NZVI and water (Bae and Hanna, 2015). After the addition of AgNPs at 10 mg/L to the  
 183 NZVI suspension, the pH and ORP values remained constant, and only slight changes  
 184 were observed in the pH and ORP after 15 h of reaction. The slight decreasing in pH  
 185 and increasing in ORP value may be attributed to the consumption of Fe<sup>2+</sup> and OH<sup>-</sup> by

186 the hydrolysis of ferrous under alkaline conditions (Deng et al., 2020). Afterward, little  
187 variations in pH or ORP were observed during the *p*-NP removal. Only a slight decrease  
188 in pH and increase in ORP was observed upon the addition of the *p*-NP solution.

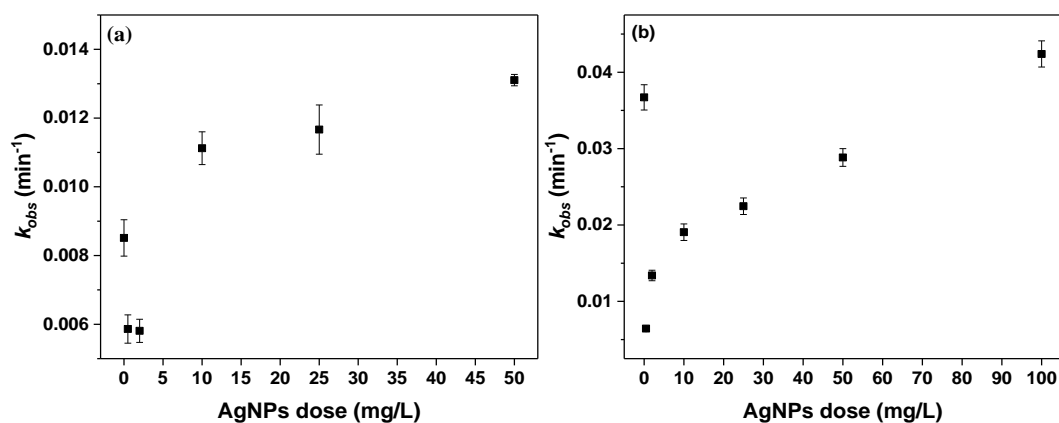
189 The removal of *p*-NP by various materials, including NZVI alone, AgNPs alone,  
190 and NZVI/AgNPs mixture, was also evaluated (Fig. 1). Since the standard potential of  
191  $\text{Ag}^0/\text{Ag}^+$  and *p*-NP/*p*-AP is 0.79 V and 0.76 V respectively, the conversion of *p*-NP to  
192 *p*-AP by AgNPs is not likely to take place spontaneously (Hernández-Gordillo et al.  
193 2014). Indeed, no *p*-NP removal was observed in the AgNP suspension, which indicated  
194 negligible adsorption and/or reduction of *p*-NP by AgNPs. In contrast, the complete  
195 removal of *p*-NP was observed after 90 min of reaction with NZVI, whereas 85% of *p*-  
196 NP was removed by the NZVI-AgNP suspension over 120 min. The mass balance was  
197 evaluated, which confirmed the reductive conversion of *p*-NP to *p*-AP (not shown) and  
198 the negligible adsorption of *p*-NP and *p*-AP on the NZVI surface. It is reported that the  
199 hydrogen production caused by anaerobic corrosion of NZVI could potentially affect  
200 the reduction of target contaminants (Liu and Lowry, 2006). However, the working pH  
201 was 9 in our experiments, which significantly decrease the generation of hydrogen gas  
202 (Liu and Lowry 2006). In addition, it has been generally accepted that the active H atom  
203 seems to be readily captured by reactive catalysts (e.g., Ni) rather than Fe phase, and  
204 reduction of *p*-NP could not be occurred by dissolved hydrogen alone (Du et al. 2004).  
205 Therefore, hydrogen contribution should be of minor importance in our reaction  
206 systems.

207 The effect of varying AgNP concentrations (0.5–100 mg/L) on the *p*-NP removal  
208 by NZVI (25 and 50 mg/L) was then investigated (Fig. S2). Nearly 72% of *p*-NP was  
209 removed by 25 mg/L of NZVI after 8 h, whereas the addition of 0.5 mg/L of AgNPs to  
210 the NZVI suspension decreased the removal to 62%. An increase in the AgNP  
211 concentration resulted in a gradual increase in the conversion of *p*-NP to *p*-AP (i.e., 64%  
212 at 2 mg/L, 84% at 10 mg/L, 89% at 25 mg/L, and 93% at 50 mg/L) (Fig. S2(a)).  
213 Similarly, the removal efficiency of *p*-NP after 2 h of reaction significantly decreased  
214 when 0.5 mg/L of AgNPs was added to a 50 mg/L NZVI suspension, and it continuously  
215 increased as the AgNP content increased (Fig. S2(b)).

216 To further demonstrate the variations in removal rate, we plotted the removal  
217 kinetics fitted using the pseudo-first-order equation over the early reaction stage (60  
218 min) and the removal rate constants ( $k_{obs}$ ) against AgNP dose (Fig. 2 and Fig. S2(c) and  
219 (d)). Compared to NZVI alone (0.0085 min<sup>-1</sup> at 25 mg/L, and 0.037 min<sup>-1</sup> at 50 mg/L),  
220 the obtained rate constant was nearly 1.5 and 5.8 times lower after the addition of 0.5  
221 mg/L AgNPs. However, the  $k_{obs}$  values gradually increased to 0.0131 and 0.042 min<sup>-1</sup>  
222 as the AgNP dose increased, at 25 and 50 mg/L NZVI, respectively. Therefore, the  
223 results showed that the presence of AgNPs at a low dose significantly inhibited the  
224 NZVI reactivity, but this inhibitive effect gradually disappeared as the AgNP  
225 concentration increased.

226 To verify whether this two-step phenomenon was specific to AgNPs, additional  
227 investigations were conducted with nanosized TiO<sub>2</sub> particles (used as active

228 nanoparticles) and microsized quartz sand particles (used as an inert surface) under dark  
229 conditions. For TiO<sub>2</sub>, the inhibition of *p*-NP removal was observed at a low dosage (5  
230 mg/L), whereas an increase in TiO<sub>2</sub> dose enhanced the *p*-NP reduction (Fig. S3). It is  
231 worth noting that TiO<sub>2</sub> alone showed negligible removal of *p*-NP at pH 9 (See Fig. S4),  
232 suggesting that possible adsorption of *p*-NP on TiO<sub>2</sub> can be excluded under our  
233 experimental conditions. However, the addition of quartz sand showed a one-step  
234 behavior, that is, the removal rate constant continuously increased with increasing sand  
235 dose (Fig. S5). Collectively, these results suggest that the increase or decrease in *p*-NP  
236 removal rate was not limited to the effect of AgNPs, and it likely resulted from a  
237 combination of physical and chemical processes.



238  
239 Figure 2. Variation in pseudo-first-order kinetic rate constants ( $k_{obs}$ ,  $\text{min}^{-1}$ ) of the  
240 removal of *p*-NP by NZVI with respect to AgNP dosage at (a) 25 mg/L NZVI and (b)  
241 50 mg/L NZVI. Experimental conditions:  $[p\text{-NP}]_{\text{initial}} = 0.1 \text{ mM}$ ;  $\text{pH} = 9.0 \pm 0.2$ .

242

### 243 3.2 Heteroaggregation and homoaggregation of AgNPs

244 The kinetic experiments suggested that the NZVI reactivity can be altered by the  
245 interactions between AgNPs and NZVI, which might be caused by potential  
246 aggregation and/or redox reactions between the two particles. As previously observed  
247 for goethite and hematite (Wang et al., 2019), AgNPs might bind to the surface of the  
248 oxides layer in the core-shell structure of NZVI. Accordingly, the electrostatic attraction  
249 between negatively charged AgNPs (PZC  $\sim$ 3.3) and iron oxides has been used to  
250 explain the heteroaggregation process and inhibition of AgNP dissolution (Wang et al.,  
251 2019). However, these interactions have been investigated at circumneutral pH values  
252 (5.5 and 7.5), at which the surface charge of goethite (PZC  $\sim$  9) and hematite (PZC  $\sim$  8)  
253 are predominately positive. This emphasizes the role of electrostatic attraction for the  
254 adsorption of negatively charged AgNPs onto iron oxides. The zeta potential of NZVI  
255 and AgNPs at different pHs were measured to gain more insight into electrostatic  
256 interactions between the two types of particle (Fig. S6). However, the working pH of  
257 the NZVI suspension lay at 9, at which the surface charge of both NPs are negative.  
258 Indeed, at pH above the PZC of minerals, dissociation of surface functional groups in  
259 water will give a negatively charged surface (Lützenkirchen et al. 2008).

260 To investigate the interparticle interactions in NZVI-AgNP suspensions under the  
261 experimental conditions of the present work, TEM-EDS analyses were conducted. The  
262 silver nanoparticles sample used in this study is mostly round shape with particle size  
263 in water lower than 100 nm. The NZVI showed chain-like aggregates consisting of  
264 spherical particles (60–100 nm) (Fig. 3(a)), which are generally attributed to the high

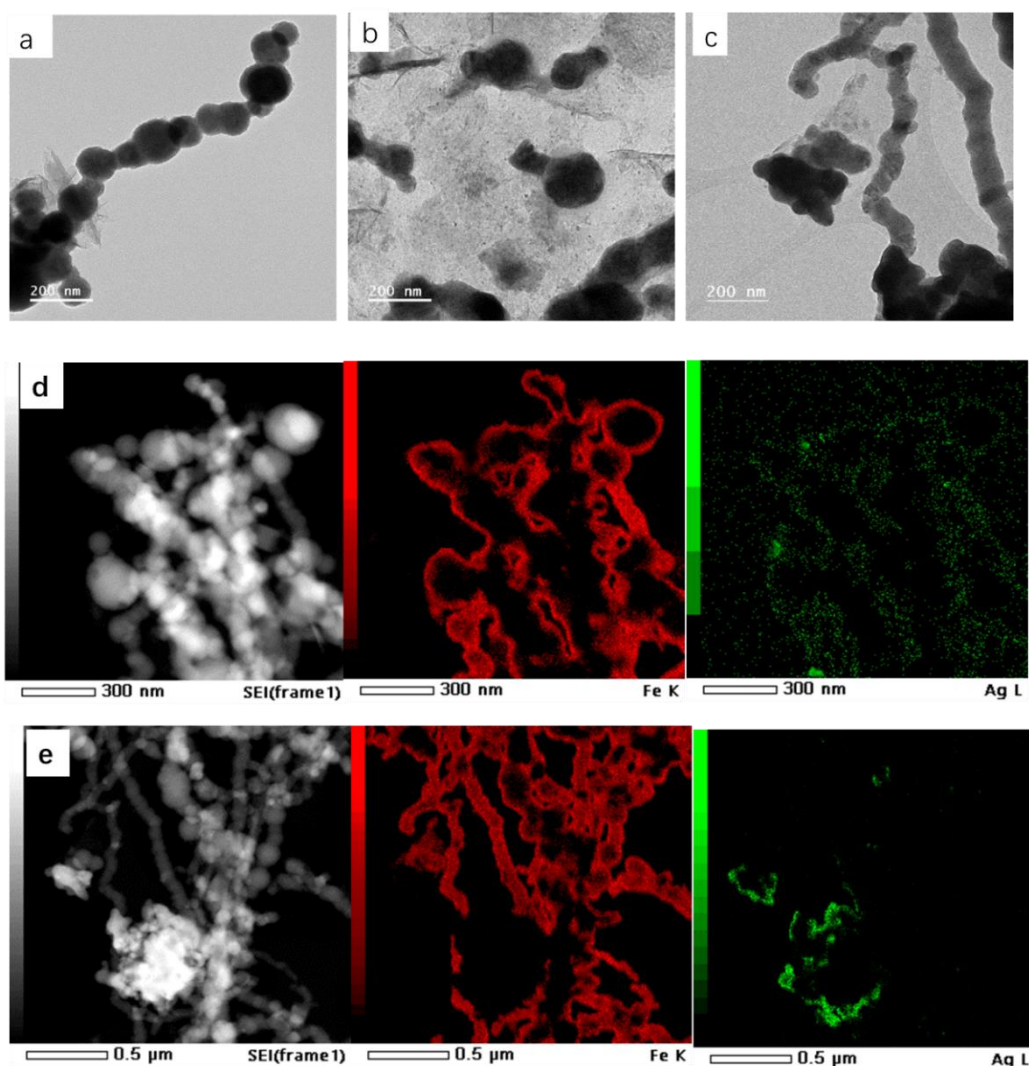
265 surface energy and intrinsic magnetic interaction among NZVI particles (Sohn et al.,  
266 2006). Significantly smaller particles were attached to larger particles (80–100 nm)  
267 when 10 mg/L of AgNPs was added (Fig. 3(b)). However, the attachment of small  
268 particles was not observed at a high AgNP dose (100 mg/L) (Fig. 3(c)). Instead, we  
269 observed the co-existence of chain-like aggregates and nanoparticle assemblages. The  
270 EDS mapping of NZVI-AgNP mixtures showed distinct Fe and Ag nanoparticles  
271 highlighted in red and green, respectively, in Figs. 3(d) and (e). As illustrated in Fig.  
272 3(d), the Ag-phase was enriched near the surface of Fe aggregates at low AgNP  
273 concentrations, which suggests the heteroaggregation of NZVI and AgNPs. The spatial  
274 correlation of Ag and Fe was not observed at high AgNP concentrations (Fig. 3(e)), but  
275 these two elements existed in different locations because AgNPs tended to  
276 homoaggregate rather than interact with NZVI at higher AgNP doses. It was previously  
277 reported that aggregation behavior of NPs would change along with their oxidation  
278 (Vilardi 2019, Vilardi et al. 2019). However, similar TEM images of AgNPs and NZVI  
279 were observed after the reaction with *p*-NP (Fig. S7), suggesting no significant  
280 modification of the interactions between NZVI and AgNPs.

281 The enlarged TEM images with EDS mapping revealed a clear difference for  
282 different AgNP dosages (Fig. S8). In the absence of AgNPs (Fig. S8(a)), the TEM  
283 images of NZVI showed a typical shape of NZVI particles covered by a thin Fe oxide  
284 shell. The corresponding elemental mapping (Fe and O) further displayed the core-shell  
285 structure of NZVI, showing a strong signal intensity of Fe in the core, whereas O was



286 mostly present in the shell layer (2.5–3.5 nm). However, the thickness of the NZVI  
287 oxide shell seems to decrease significantly after the addition of 100 mg/L AgNPs,  
288 whereas almost no change was observed with the addition of 10 mg/L AgNPs. Based  
289 on the TEM–EDS results, we hypothesized that AgNPs at a low dose attach to the NZVI  
290 surfaces (i.e., iron oxides), and at a high dose, they tend to homoaggregate. We also  
291 hypothesized that introducing a high dosage of AgNP would lead to a decrease in the  
292 thickness of the NZVI oxide layer, which should be further investigated.

293



294 Figure 3. TEM images of (a) NZVI, (b) AgNP–NZVI at 10 mg/L AgNPs, and (c)

295 AgNP–NZVI at 100 mg/L AgNPs. Elemental mapping of AgNP–NZVI at AgNP doses  
296 of (d) 10 mg/L and (e) 100 mg/L. Conditions: [NZVI] = 50 mg/L.

297

298 We also analyzed the attraction and repulsion behaviors of AgNPs and NZVI  
299 according to the DLVO theory. This theory considers attractive van der Waals (vdW)  
300 and repulsive electrostatic double-layer (EDL) forces between the particles ( $\Phi_{DLVO} =$   
301  $\Phi_{EDL} + \Phi_{vdW}$ ). The details of DLVO calculations are provided in the SI. In brief, at a low  
302 AgNP dose (10 mg/L), heteroaggregation (AgNP–NZVI) is likely to occur because of  
303 the lower repulsive energy barriers of AgNP–NZVI with respect to AgNP–AgNP. In  
304 addition, the AgNPs used in this study also contained stabilized PVP, so the surface  
305 coatings could serve as a bridge between coated AgNPs and uncoated NZVI to  
306 overcome the energy barrier (Lin et al., 2012). Therefore, it is likely that PVP-stabilized  
307 AgNPs formed heteroaggregates with NZVI. In contrast, a higher AgNP dose (100  
308 mg/L) led to a significantly higher magnitude of calculated maximum repulsive  
309 interaction energies ( $\Phi_{max}$ ), which would not be sufficient to overcome non-DLVO  
310 energy. According to the calculations, neither heteroaggregation nor homoaggregation  
311 (AgNP–AgNP) would occur spontaneously. However, AgNP homoaggregation was  
312 still observed using TEM–EDS. This discrepancy between DLVO calculations and  
313 TEM images might be attributed to the potential chemical interactions between AgNPs  
314 and NZVI or oxide layer coating NZVI.

315 A recent study reported that AgNP morphology may change from a dispersed

316 spherical shape to larger aggregates owing to the release of  $\text{Ag}^+$  possibly because of (i)  
317 the nano bridges created by adsorption and/or redox conversion of  $\text{Ag}^+$  into  $\text{Ag}^0$  at the  
318 particle surface to connect nearby particles, and (ii) the growth of reformed small  
319 AgNPs around old AgNPs (Yu et al., 2014). Other reports showed that  $\text{Ag}^+$  released  
320 from AgNPs and possible electron transfer from  $\text{Fe}^0$  to  $\text{Ag}^+$  could form a galvanic  
321 couple, which may accelerate NZVI-water corrosion (Zhuang et al., 2011; Zhu et al.,  
322 2021). Therefore, interactions of  $\text{Ag}^+$  ions ( $E_0 \text{Ag}/\text{Ag}^+ 0.799 \text{ V}$ ) with NZVI ( $E_0 \text{Fe}/\text{Fe}^{2+}$   
323  $0.44 \text{ V}$ ) and AgNPs through adsorption and/or electron transfer processes may alter the  
324 particle aggregation behavior and surface reactivity. In the present work, we have  
325 measured  $\text{Ag}^+$  ions in AgNP aqueous suspension but in the absence of NZVI, to avoid  
326 sorption of released  $\text{Ag}^+$  ions on iron oxide layer of NZVI surface. As a result, these  
327 dissolution tests were performed under oxic (open atmosphere) or mild reducing  
328 conditions (anaerobic chamber), since the strong reducing conditions are ensured by  
329 the presence of NZVI. Under such conditions,  $\text{Ag}^+$  can be detected, and released  
330 concentration was increased with increasing AgNP dose (See Fig. S10). However,  
331 examination of the thermodynamic database by means of Eh-pH diagrams of Ag species  
332 suggests that ions released through metal corrosion should be very limited, or even  
333 excluded, under the experimental conditions of this study (pH 9, -800 mV) (Brookins,  
334 1988). Indeed, no ions can be detected at alkaline pH values and strongly reducing  
335 conditions, thereby ruling out galvanic effects between  $\text{Ag}^+$  ions and inner  $\text{Fe}^0$  within  
336 iron oxide shell. In addition, the same two-step behavior in NP removal kinetics by

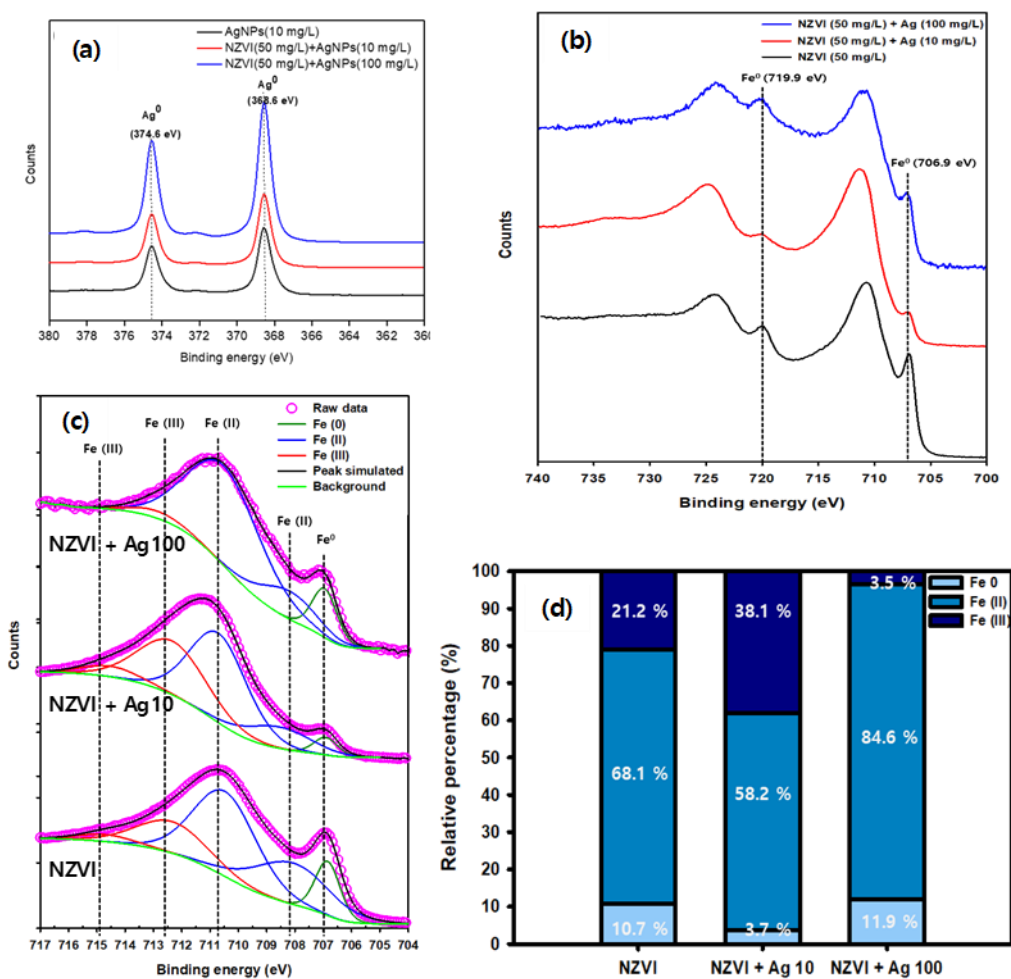
337 NZVI was observed when AgNP has been replaced by TiO<sub>2</sub> (Fig. S3), further  
338 confirming the minor role of ions release and/or galvanic effect in the investigated  
339 systems.

340 Collectively, these results suggest that heteroaggregation of NZVI-AgNPs which  
341 is favorable at lower AgNP dose owing to the relatively lower energy barrier may alter  
342 the NZVI reactivity. As the AgNP dose increased, AgNP homoaggregation can be  
343 expected, thereby preventing potential alteration of the initial NZVI reactivity.

344

### 345 *3.3. Spectroscopic investigations*

346 To investigate the oxidation states of Ag and Fe in AgNP and NZVI suspensions,  
347 the XPS spectra of the Ag(3d) and Fe(2p) bands of AgNP, NZVI, and NZVI-AgNP  
348 suspensions were analyzed (Fig. 4). For AgNPs and NZVI-AgNPs, the Ag(3d<sub>5/2</sub>) and  
349 Ag(3d<sub>3/2</sub>) peaks at 368.6 and 374.6 eV were assigned to Ag(0) (Fig. 4(a)) (Xu et al.,  
350 2011), and the splitting of the 3d doublet of Ag (6.0 eV) confirmed the presence of Ag(0)  
351 (Chastain and King Jr, 1992; Xu et al., 2011).



352

353 Figure 4. XPS spectra of (a) Ag(3d) in AgNP and NZVI-AgNP suspensions, (b) Fe(2p)

354 in NZVI and NZVI-AgNP suspensions, (c) the corresponding deconvolution results of

355 Fe(2p<sub>3/2</sub>) (705–717 eV), and (d) relative percentage of iron species.

356

357 In the pristine NZVI, two distinct peaks were observed at 719.9 and 706.9 eV,

358 which corresponded to the Fe(2p<sub>1/2</sub>) and Fe(2p<sub>3/2</sub>) of Fe(0) (Luo et al., 2014),

359 respectively (Fig. 4(b)). In the NZVI-AgNP suspension, Fe(0) peaks were enhanced,

360 indicating the presence of more Fe(0) on the NZVI surface after AgNPs were introduced

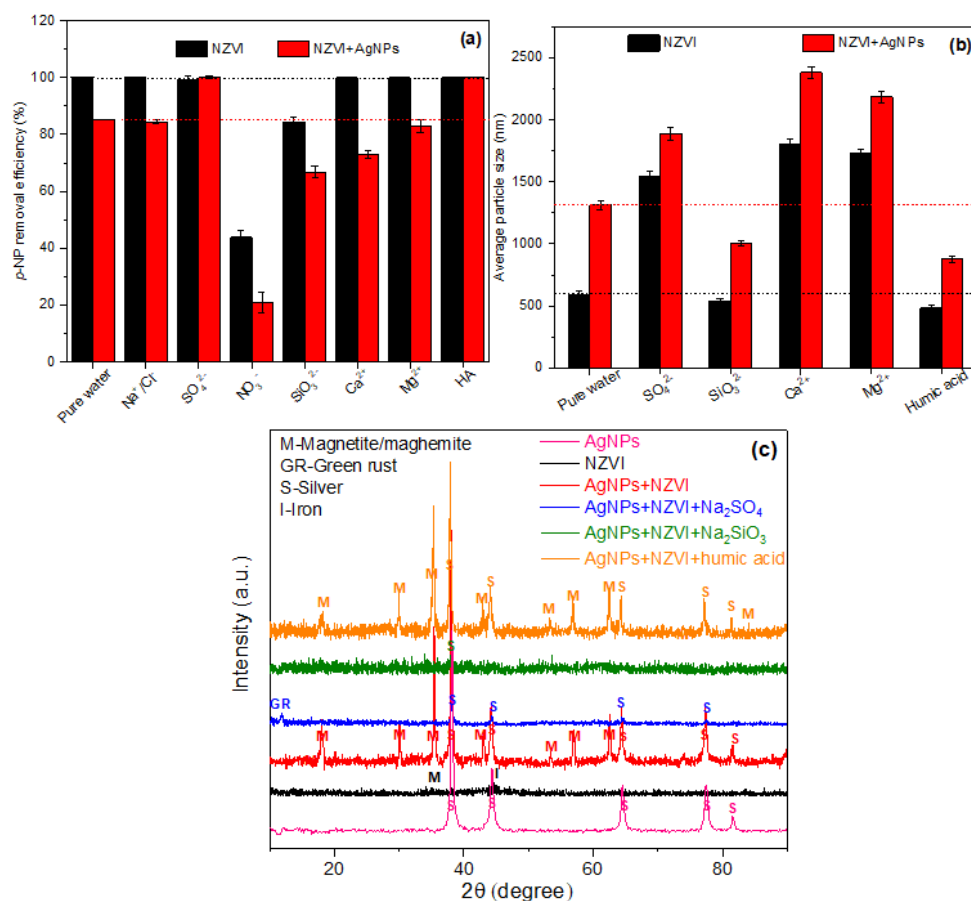
361 (Li et al., 2009). The XPS spectra of Fe(2p<sub>3/2</sub>) (Fig. 4(c)) showed five peaks at 706.9,

362 708.2–708.5, 710.3–710.7, 711.5–711.6, and 713.1–713.7 eV, which were assigned to  
363 the binding energies of Fe(0) (706.5–707.0 eV), Fe(II)–O (708.2–710.9 eV), and  
364 Fe(III)–O (711.0–714.0 eV). The proportion of Fe(0) (10.7%) and Fe(II) (68.1%) on  
365 the NZVI surfaces significantly decreased to 3.7% and 58.2% after adding 10 mg/L  
366 AgNPs, respectively (Fig. 4(d)). In contrast, their percentages dramatically increased  
367 to 11.9% and 84.6% in the sample of NZVI with 100 mg/L AgNPs. These results  
368 demonstrate that the presence of AgNPs decreased and increased the Fe(0) content on  
369 the NZVI surface, which are in agreement with the results of degradation kinetics in  
370 Fig. 2(b). This is also consistent with the TEM–EDS results (Fig. S8(c)), which showed  
371 a thinner oxide layer on the NZVI surface at a higher AgNP dose. Previous  
372 investigations have shown that the collision and friction between particles might occur  
373 in suspensions under stirring conditions (Xie and Luo, 2018). In addition, these particle-  
374 particle interactions become much stronger when both particle size and solid loading  
375 increased (Xie and Luo, 2018). In our systems, higher AgNP doses enabled  
376 homoaggregation and an increase in aggregate size (Fig. S11), likely inducing more  
377 collision between large-sized AgNP aggregates and NZVI. This phenomenon likely  
378 contributed to the peeling of the NZVI surface layer, which further resulted in the  
379 exposure of the NZVI inner core. These results suggest that a higher AgNP dose led to  
380 the partial removal of the iron oxide shell of NZVI through collisions between AgNP  
381 homoaggregates and NZVI. Self-assembled AgNPs with bigger sizes accelerated the  
382 peeling of the Fe oxide shell on the NZVI surface, thereby increasing the exposure of

383 inner Fe(0), and consequently, enhancing the *p*-NP removal. This also explains the  
 384 enhanced NZVI reactivity under an increasing dose of sand microparticles (Fig. S5).  
 385 As sand microparticles are inert and have a low surface area (0.06 m<sup>2</sup>/g), the enhanced  
 386 NZVI reductive ability may be attributed to collision-driven processes in an aqueous  
 387 suspension.

388

389 *3.4. Effects of groundwater constituents on nanoparticles interaction and reactivity*



390

391 Figure 5. (a) Removal efficiencies of *p*-NP (2 h reaction) by NZVI and NZVI+AgNPs  
 392 in the presence of co-existing groundwater solutes; (b) Average particle size of NZVI

393 and AgNP–NZVI complexes in the presence of non-competing groundwater solutes; (c)  
394 XRD pattern of the resulting products after the reaction of *p*-NP with non-competing  
395 groundwater solutes. Experimental conditions: [*p*-NP]<sub>initial</sub> = 0.1 mM; [NZVI] = 50  
396 mg/L; [AgNPs] = 10 mg/L; pH = 9.0±0.2; [Na<sup>+</sup>/Cl<sup>-</sup>] = 5 mM; [SO<sub>4</sub><sup>2-</sup>] = 1 mM; [NO<sub>3</sub><sup>-</sup>]  
397 = 0.5 mM; [SiO<sub>3</sub><sup>2-</sup>] = 0.5 mM; [Ca<sup>2+</sup>] = 2 mM; [Mg<sup>2+</sup>] = 2 mM; and [HA] = 5 mg/L.

398

399 In the environment, the concentration of AgNPs is normally much lower than those  
400 of NZVI used for remediation purposes (Su et al., 2013; McGillicuddy et al., 2018), the  
401 inhibition effect of AgNPs to NZVI would be more significant in natural systems. To  
402 evaluate the inhibition effects of AgNPs on the NZVI reactivity in conditions that  
403 emulate natural systems, the *p*-NP reduction in NZVI (50 mg/L) and AgNP (10 mg/L)  
404 suspensions was investigated in the presence of naturally occurring cations, anions, and  
405 organic matter. Experiments were conducted with groundwater constituents and humic  
406 acids (HAs) at levels similar to those encountered in real groundwater (Fig. 5(a))  
407 (Edmunds and Shand, 2008). No impact of NaCl was observed. In the presence of most  
408 groundwater solutes, NZVI exhibited good performance for *p*-NP removal, with 100%  
409 removal over 2 h, except in the presence of NO<sub>3</sub><sup>-</sup> (44%) and SiO<sub>3</sub><sup>2-</sup> (84%). For NO<sub>3</sub><sup>-</sup>,  
410 the inhibitive result could be caused by a competitive reduction of NO<sub>3</sub><sup>-</sup> by NZVI (Ryu  
411 et al., 2011). Compared to NZVI-AgNPs in pure water (85%), the removal efficiency  
412 of *p*-NP by the NZVI-AgNPs with NO<sub>3</sub><sup>-</sup>, SiO<sub>3</sub><sup>2-</sup>, Ca<sup>2+</sup>, and Mg<sup>2+</sup> decreased to 21%, 67%,  
413 73%, and 83%, respectively. Furthermore, *p*-NP was completely removed over 2 h in



414 the presence of  $\text{SO}_4^{2-}$  and HA, which represents a better performance than that obtained  
415 in pure water.

416 To further clarify the aggregation behavior of the particles, we measured the  
417 average particle sizes of NZVI and AgNP–NZVI suspensions in the presence of  $\text{SO}_4^{2-}$ ,  
418  $\text{SiO}_3^{2-}$ ,  $\text{Ca}^{2+}$ ,  $\text{Mg}^{2+}$ , and HA (Fig. 5(b)). As expected, the particles sizes in the NZVI-  
419 AgNP systems were higher than in systems without AgNPs, which was attributed to the  
420 heteroaggregation between AgNPs and NZVI particles. Upon the introduction of  $\text{Ca}^{2+}$   
421 or  $\text{Mg}^{2+}$ , the particle size drastically increased from 593 nm to 1804 and 1727 nm in the  
422 NZVI system, and from 1313 nm to 2382 and 2186 nm in the NZVI-AgNP system,  
423 respectively. This was attributed to the particle surface charge screening (EDL  
424 contraction) by  $\text{Ca}^{2+}/\text{Mg}^{2+}$  (Rogozhnikov, 2001). EDL contraction can decrease the  
425 electrostatic or steric repulsive forces of the nanoparticles, thereby increasing  
426 aggregation (Petosa et al., 2010) and further decreasing the NZVI reactivity (Ryu et al.,  
427 2011). Moreover,  $\text{Ca}^{2+}$  and  $\text{Mg}^{2+}$  showed stronger inhibitive effects in NZVI-AgNPs  
428 than in NZVI alone. In the presence of  $\text{Ca}^{2+}$  or  $\text{Mg}^{2+}$ , electrostatic repulsive forces  
429 among particles (i.e., NZVI–NZVI, NZVI–AgNP, AgNP–AgNP) favored  
430 homoaggregation and heteroaggregation, thus altering the NZVI reactivity.

431 In contrast, a decrease in the average particle size of NZVI (from 593 to 486 nm)  
432 and NZVI-AgNPs (from 1313 to 877 nm) in the presence of HA was attributed to the  
433 interactions of HA with the surfaces, which likely enhanced the electrostatic repulsion  
434 decreased (Dong and Lo, 2013). This reduced particle aggregation, which enhanced the

435 removal of *p*-NP. The particle size decreased more for NZVI-AgNPs than for NZVI,  
436 which suggests that less AgNPs were attached to NZVI surfaces, thereby providing a  
437 lower inhibition effect of AgNPs in the presence of HA.

438 XRD analysis was also conducted to analyze the passivation byproducts of NZVI-  
439 AgNPs after the reaction (Fig. 5(c)). The byproducts in the pure water system included  
440 maghemite ( $\gamma$ -Fe<sub>2</sub>O<sub>3</sub>)/magnetite (Fe<sub>3</sub>O<sub>4</sub>) and silver (Ag(0)), which were attributed to  
441 NZVI oxidation during the *p*-NP reduction (Xiong et al., 2018). Similarly, in the  
442 presence of HA, maghemite/magnetite and silver (Ag(0)) phases were also detected  
443 after *p*-NP removal. In contrast, green rust ( $[\text{Fe}^{2+}_4\text{Fe}^{3+}_2(\text{HO}^-)_{12}]^{2+} \cdot [\text{SO}_4^{2-} \cdot 2\text{H}_2\text{O}]^{2-}$ )  
444 (Tahawy et al., 2021) and silver (Ag(0)) were detected in the presence of SO<sub>4</sub><sup>2-</sup>.  
445 Considering the relatively higher reactivity of green rust than that of magnetite  
446 (Digiacomo et al., 2020; Usman et al., 2018), the enhanced *p*-NP removal in the NZVI-  
447 AgNP-SO<sub>4</sub><sup>2-</sup> system (Fig. 5(a)) was attributed to the generated green rust. For SiO<sub>3</sub><sup>2-</sup>, a  
448 weak peak of silver was identified as the final product, and there was no obvious Fe  
449 phase detected in the XRD analysis. The absence of Fe phases might be attributed to  
450 the amorphous coating of Si on the NZVI surface as previously reported, and the surface  
451 coated Si would further reduce the amount of active surface sites available for  
452 contaminants (Meng et al., 2002). Despite the lower particle size of NZVI-AgNP-SiO<sub>3</sub><sup>2-</sup>,  
453 the reactivity of both NZVI and NZVI/AgNPs decreased drastically, which was  
454 attributed to the strong binding of silicates to the NZVI surface.

#### 455 4. Conclusions

456 Because of the increasing use of engineered nanoparticles (ENPs) in various  
457 industries and consumer items, ENPs are ubiquitously found in aquatic environments.  
458 However, little is known about the interactions among the co-existing ENPs in nature.  
459 This work showed for the first time how two typical engineered nanoparticles,  
460 nanoscale zero-valent iron (NZVI) and silver nanoparticles (AgNPs), interact and  
461 influence each other under environmentally-relevant conditions. First, we have  
462 investigated the potential interactions between AgNPs and NZVI particles using *p*-NP  
463 conversion into *p*-AP as a probe reaction. At a AgNP load of 10 mg/L, AgNPs covered  
464 the reactive NZVI surfaces, which decreased *p*-NP removal. Whereas at a AgNP load  
465 of 100 mg/L, the enhanced homoaggregation of AgNPs led to the exposure of the inner  
466 Fe(0) surface of NZVI because of particle collisions, which increased the *p*-NP removal.  
467 The same behavior was observed with nanosized TiO<sub>2</sub> particles and microsized quartz  
468 sand particles, thereby excluding the role of potential Ag<sup>+</sup> ions release, electron transfer  
469 process, and/or galvanic effect.

470 Second, the impact of groundwater constituents has been evaluated, which showed  
471 contrasting effects depending on ion types and the binding affinities to Fe-oxides. These  
472 results revealed that not only AgNPs but also other nano/microsized particles (e.g. TiO<sub>2</sub>  
473 and quartz sand) may influence the NZVI reactivity, which will help to develop decision  
474 support and prediction tools for NZVI remediation technologies. Electron microscopic  
475 and X-ray spectroscopic investigations and DLVO calculations revealed that  
476 heteroaggregation of NZVI and AgNPs resulted in dramatic decrease of the NZVI

477 reactivity, while at higher AgNPs loading, collision between self-assembled aggregates  
478 of AgNPs and NZVI can improve the reductive ability of NZVI. These findings shed  
479 light on an overlooked aspect of interactions between co-existing nanoparticles, which  
480 could influence their fate and mobility in environmental settings. Owing to the  
481 increasing occurrence of NPs in aqueous environments, this work calls for more  
482 investigations of potential interactions between the co-occurring nanomaterials for  
483 accurate assessment of environmental associated risks.

#### 484 **Conflicts of interest**

485 There are no conflicts to declare.

#### 486 **Acknowledgments**

487 We would like to acknowledge the support from Korea Environment Industry &  
488 Technology Institute (KEITI) through “Subsurface Environmental Management (SEM)  
489 Project”, funded by Korea Ministry of Environment (MOE) (2020002480006). We are  
490 also grateful for the assistance of Isabelle Soutrel (LC/UV) and Vincent Dorcet  
491 (THEMIS platform).

492

493

494 **References**

- 495 Abbas, Q., Yousaf, B., Amina, Ali, M.U., Munir, M.A.M., El-Naggar, A., Rinklebe, J.,  
496 Naushad, M., 2020. Transformation pathways and fate of engineered nanoparticles  
497 (ENPs) in distinct interactive environmental compartments: A review. *Environ. Int.* 138,  
498 105646.
- 499 Asghari, S., Johari, S.A., Ji, H.L., Yong, S.K., Yong, B.J., Choi, H.J., Min, C.M., Yu,  
500 I.J., 2012. Toxicity of various silver nanoparticles compared to silver ions in *Daphnia*  
501 *magna*. *J. Nanobiotechnology* 10(1), 1-11.
- 502 Auffan, M., Pedetour, M., Rose, J., Masion, A., Ziarelli, F., Borschneck, D., Chaneac,  
503 C., Botta, C., Chaurand, P., Labille, J., Bottero, J.-Y., 2010. Structural Degradation at  
504 the Surface of a TiO<sub>2</sub>-Based Nanomaterial Used in Cosmetics. *Environ. Sci. Technol.*  
505 44(7), 2689-2694.
- 506 Bae, S., Gim, S., Kim, H., Hanna, K., 2016. Effect of NaBH<sub>4</sub> on properties of nanoscale  
507 zero-valent iron and its catalytic activity for reduction of p-nitrophenol. *Appl. Catal., B*  
508 182, 541-549.
- 509 Bae, S., Hanna, K., 2015. Reactivity of nanoscale zero-valent iron in unbuffered  
510 systems: effect of pH and Fe (II) dissolution. *Environ. Sci. Technol.* 49(17), 10536-  
511 10543.
- 512 Bae, S., Lee, W., 2014. Influence of Riboflavin on Nanoscale Zero-Valent Iron  
513 Reactivity during the Degradation of Carbon Tetrachloride. *Environ. Sci. Technol.*  
514 48(4), 2368-2376.
- 515 Brookins D.G. Eh- pH diagrams of geochemistry. Springer-Verlag, New York (1988).
- 516 Chastain, J., King Jr, R.C., 1992. Handbook of X-ray photoelectron spectroscopy.  
517 Perkin-Elmer Corporation 40, 221.
- 518 Danail, H., Ineke, M., 2009. Hazards and Risks of Engineered Nanoparticles for the  
519 Environment and Human Health. *Sustainability* 1(4), 1161-1161.
- 520 Deng, H., McShan, D., Zhang, Y., Sinha, S.S., Arslan, Z., Ray, P.C., Yu, H., 2016.  
521 Mechanistic study of the synergistic antibacterial activity of combined silver  
522 nanoparticles and common antibiotics. *Environ. Sci. Technol.* 50(16), 8840-8848.
- 523 Deng, J., Bae, S., Yoon, S., Pasturel, M., Marsac, R., Hanna, K., 2020. Adsorption  
524 capacity of the corrosion products of nanoscale zerovalent iron for emerging  
525 contaminants. *Environ. Sci. Nano* 7(12), 3773-3782.
- 526 Digiacomo, F., Tobler, D.J., Held, T., Neumann, T., 2020. Immobilization of Cr(VI) by  
527 sulphate green rust and sulphidized nanoscale zerovalent iron in sand media: batch and  
528 column studies. *Geochem. Trans.* 21(1), 8.

529 Dong, H., Lo, I.M.C., 2013. Influence of humic acid on the colloidal stability of surface-  
530 modified nano zero-valent iron. *Water Res.* 47(1), 419-427.

531 Du, Y., Chen, H., Chen, R., Xu, N. 2004. Synthesis of p-aminophenol from p-  
532 nitrophenol over nano-sized nickel catalysts. *Appl. Catal. A-Gen* 277(1), 259-264.

533 Echegoyen, Y., Nerín, C., 2013. Nanoparticle release from nano-silver antimicrobial  
534 food containers. *Food Chem. Toxicol.* 62, 16-22.

535 Edmunds, W.M., Shand, P., 2008. Natural groundwater quality.

536 Hernández-Gordillo, A., Arroyo, M., Zanella, R., Rodríguez-González, V. 2014.  
537 Photoconversion of 4-nitrophenol in the presence of hydrazine with AgNPs-TiO<sub>2</sub>  
538 nanoparticles prepared by the sol-gel method. *J. Hazard. Mater.* 268, 84-91.

539 Joo, S.H., Feitz, A.J., Waite, T.D., 2004. Oxidative Degradation of the Carbothioate  
540 Herbicide, Molinate, Using Nanoscale Zero-Valent Iron. *Environ. Sci. Technol.* 38(7),  
541 2242-2247.0.799

542 Lai, B., Zhang, Y.-H., Li, R., Zhou, Y.-X., Wang, J., 2014. Influence of operating  
543 temperature on the reduction of high concentration p-nitrophenol (PNP) by zero valent  
544 iron (ZVI). *Chem. Eng. J.* 249, 143-152.

545 Li, S., Wang, W., Liang, F., Zhang, W.-x., 2017. Heavy metal removal using nanoscale  
546 zero-valent iron (nZVI): Theory and application. *J. Hazard. Mater.* 322, 163-171.

547 Li, S., Yan, W., Zhang, W.-x., 2009. Solvent-free production of nanoscale zero-valent  
548 iron (nZVI) with precision milling. *Green Chem.* 11(10), 1618-1626.

549 Lin, S., Cheng, Y., Liu, J., Wiesner, M.R., 2012. Polymeric Coatings on Silver  
550 Nanoparticles Hinder Autoaggregation but Enhance Attachment to Uncoated Surfaces.  
551 *Langmuir* 28(9), 4178-4186.

552 Liu, Y., Lowry, G.V., 2006. Effect of Particle Age (Fe<sub>0</sub> Content) and Solution pH On  
553 NZVI Reactivity: H<sub>2</sub> Evolution and TCE Dechlorination. *Environ. Sci. Technol.*  
554 40(19), 6085-6090.

555 Lorenz, C., Windler, L., von Goetz, N., Lehmann, R.P., Schuppler, M., Hungerbühler,  
556 K., Heuberger, M., Nowack, B., 2012. Characterization of silver release from  
557 commercially available functional (nano)textiles. *Chemosphere* 89(7), 817-824.

558 Luo, S., Lu, T., Peng, L., Shao, J., Zeng, Q., Gu, J.-D., 2014. Synthesis of nanoscale  
559 zero-valent iron immobilized in alginate microcapsules for removal of Pb(II) from  
560 aqueous solution. *J. Mater. Chem. A* 2(37), 15463-15472.

561 Lützenkirchen, J., Preočanin, T. and Kallay, N. 2008. A macroscopic water structure  
562 based model for describing charging phenomena at inert hydrophobic surfaces in  
563 aqueous electrolyte solutions. *Phys. Chem. Chem. Phys.* 10(32), 4946-4955.

564 Mahdi, K.N.M., Peters, R.J.B., Klumpp, E., Bohme, S., Ploeg, M.v.d., Ritsema, C.,

565 Geissen, V., 2017. Silver nanoparticles in soil: Aqueous extraction combined with  
566 single-particle ICP-MS for detection and characterization. *Environ. Nanotechnol.*  
567 *Monit. Manag.* 7, 24-33.

568 McGillicuddy, E., Morrison, L., Cormican, M., Dockery, P., Morris, D., 2018. Activated  
569 charcoal as a capture material for silver nanoparticles in environmental water samples.  
570 *Sci. Total Environ.* 645, 356-362.

571 Meng, X., Korfiatis, G.P., Bang, S., Bang, K.W., 2002. Combined effects of anions on  
572 arsenic removal by iron hydroxides. *Toxicol. Lett.* 133(1), 103-111.

573 Mueller, N.C., Braun, J., Bruns, J., Černík, M., Rissing, P., Nowack, R.B., 2012.  
574 Application of nanoscale zero valent iron (NZVI) for groundwater remediation in  
575 Europe. *Environ. Sci. Pollut. Res.* 19(2), 550-558.

576 Petosa, A.R., Jaisi, D.P., Quevedo, I.R., Elimelech, M., Tufenkji, N., 2010. Aggregation  
577 and deposition of engineered nanomaterials in aquatic environments: role of  
578 physicochemical interactions. *Environ. Sci. Technol.* 44(17), 6532-6549.

579 Phenrat, T., Thongboot, T., Lowry, G.V., 2016. Electromagnetic Induction of Zerovalent  
580 Iron (ZVI) Powder and Nanoscale Zerovalent Iron (NZVI) Particles Enhances  
581 Dechlorination of Trichloroethylene in Contaminated Groundwater and Soil: Proof of  
582 Concept. *Environ. Sci. Technol.* 50(2), 872-880.

583 Poudel, M.B., Karki, H.P. and Kim, H.J. (2020) Silver nanoparticles decorated  
584 molybdenum sulfide/tungstate oxide nanorods as high performance supercapacitor  
585 electrode. *Journal of Energy Storage* 32, 101693.

586 Poudel, M.B. and Kim, H.J., 2022. Confinement of Zn-Mg-Al-layered double  
587 hydroxide and  $\alpha$ -Fe<sub>2</sub>O<sub>3</sub> nanorods on hollow porous carbon nanofibers: A free-standing  
588 electrode for solid-state symmetric supercapacitors. *Chem. Eng. J.* 429, 132345.

589 Poudel, M.B., Shin, M. and Joo Kim, H., 2022. Interface engineering of MIL-88 derived  
590 MnFe-LDH and MnFe<sub>2</sub>O<sub>3</sub> on three-dimensional carbon nanofibers for the efficient  
591 adsorption of Cr(VI), Pb(II), and As(III) ions. *Sep. Purif. Technol.* 287, 120463.

592 Poudel, M.B., Shin, M. and Kim, H.J. (2021) Polyaniline-silver-manganese dioxide  
593 nanorod ternary composite for asymmetric supercapacitor with remarkable  
594 electrochemical performance. *International Journal of Hydrogen Energy* 46(1), 474-  
595 485.

596 Rogozhnikov, N.A., 2001. Effect of Alkali Metal Cations on the EDL Structure at a  
597 Gold Electrode in Alkali Solutions. *Russ. J. Electrochem.* 37(10), 1101-1107.

598 Ryu, A., Jeong, S.-W., Jang, A., Choi, H., 2011. Reduction of highly concentrated  
599 nitrate using nanoscale zero-valent iron: Effects of aggregation and catalyst on  
600 reactivity. *Appl. Catal., B* 105(1-2), 128-135.

601 Shen, W., Zhang, X., Huang, Q., Xu, Q., Song, W., 2014. Preparation of solid silver

602 nanoparticles for inkjet printed flexible electronics with high conductivity. *Nanoscale*  
603 6(3), 1622-1628.

604 Sohn, K., Kang, S.W., Ahn, S., Woo, M., Yang, S.-K., 2006. Fe (0) nanoparticles for  
605 nitrate reduction: stability, reactivity, and transformation. *Environ. Sci. Technol.* 40(17),  
606 5514-5519.

607 Sridhar, R., Lakshminarayanan, R., Madhaiyan, K., Barathi, V.A., Lim, K.H.C.,  
608 Ramakrishna, S., 2015. Electrospayed nanoparticles and electrospun nanofibers based  
609 on natural materials: applications in tissue regeneration, drug delivery and  
610 pharmaceuticals. *Chem. Soc. Rev.* 44(3), 790-814.

611 Stefaniuk, M., Oleszczuk, P., Ok, Y.S., 2016. Review on nano zerovalent iron (nZVI):  
612 From synthesis to environmental applications. *Chem. Eng. J.* 287, 618-632.

613 Su, C., Puls, R.W., Krug, T.A., Watling, M.T., O'Hara, S.K., Quinn, J.W., Ruiz, N.E.  
614 2013. Travel distance and transformation of injected emulsified zerovalent iron  
615 nanoparticles in the subsurface during two and half years. *Water Research* 47(12), 4095-  
616 4106.

617 Syafiuddin, A., Salmiati, S., Hadibarata, T., Kueh, A.B.H., Salim, M.R., Zaini, M.A.A.,  
618 2018. Silver Nanoparticles in the Water Environment in Malaysia: Inspection,  
619 characterization, removal, modeling, and future perspective. *Sci. Rep.* 8(1), 1-15.

620 Tahawy, R., Doustkhah, E., Abdel-Aal, E.-S.A., Esmat, M., Farghaly, F.E., El-Hosainy,  
621 H., Tsunoji, N., El-Hosiny, F.I., Yamauchi, Y., Assadi, M.H.N., Ide, Y., 2021.  
622 Exceptionally stable green rust, a mixed-valent iron-layered double hydroxide, as an  
623 efficient solar photocatalyst for H<sub>2</sub> production from ammonia borane. *Appl. Catal., B*  
624 286, 119854.

625 Tsarev, S., Collins, R.N., Ilton, E.S., Fahy, A., Waite, T.D., 2017. The short-term  
626 reduction of uranium by nanoscale zero-valent iron (nZVI): role of oxide shell,  
627 reduction mechanism and the formation of U(v)-carbonate phases. *Environ. Sci. Nano*  
628 4(6), 1304-1313.

629 Usman, M., Byrne, J.M., Chaudhary, A., Orsetti, S., Hanna, K., Ruby, C., Kappler, A.,  
630 Haderlein, S.B., 2018. Magnetite and Green Rust: Synthesis, Properties, and  
631 Environmental Applications of Mixed-Valent Iron Minerals. *Chem. Rev.* 118(7), 3251-  
632 3304.

633 Vilaridi, G. 2019. Mathematical modelling of simultaneous nitrate and dissolved oxygen  
634 reduction by Cu-nZVI using a bi-component shrinking core model. *Powder Technol.*  
635 343, 613-618.

636 Vilaridi, G., Parisi, M., Verdone, N. 2019. Simultaneous aggregation and oxidation of  
637 nZVI in Rushton equipped agitated vessel: Experimental and modelling. *Powder*  
638 *Technol.* 353, 238-246.



639 Vilardi, G. 2020. P-aminophenol catalysed production on supported nano-magnetite  
640 particles in fixed-bed reactor: Kinetic modelling and scale-up. *Chemosphere* 250,  
641 126237.

642 Wang, R., Dang, F., Liu, C., Wang, D.-j., Cui, P.-x., Yan, H.-j., Zhou, D.-m., 2019.  
643 Heteroaggregation and dissolution of silver nanoparticles by iron oxide colloids under  
644 environmentally relevant conditions.. *Environ. Sci. Nano.* 6(1), 195-206.

645 Wei, Y.-T., Wu, S.-C., Chou, C.-M., Che, C.-H., Tsai, S.-M., Lien, H.-L., 2010.  
646 Influence of nanoscale zero-valent iron on geochemical properties of groundwater and  
647 vinyl chloride degradation: A field case study. *Water Res.* 44(1), 131-140.

648 Xia, X., Ling, L., Zhang, W.-x., 2017. Genesis of pure Se(0) nano- and micro-structures  
649 in wastewater with nanoscale zero-valent iron (nZVI). . *Environ. Sci. Nano* 4(1), 52-59.

650 Xie, L., Luo, Z.-H., 2018. Modeling and simulation of the influences of particle-particle  
651 interactions on dense solid–liquid suspensions in stirred vessels. *Chem. Eng. Sci.* 176,  
652 439-453.

653 Xiong, Z., Lai, B., Yang, P., 2018. Enhancing the efficiency of zero valent iron by  
654 electrolysis: Performance and reaction mechanism. *Chemosphere* 194, 189-199.

655 Xu, F., Pieltt, C., Farkas, S., Qazzaz, M., Syed, N.I., 2013. Silver nanoparticles (AgNPs)  
656 cause degeneration of cytoskeleton and disrupt synaptic machinery of cultured cortical  
657 neurons. *Mol. Brain* 6(1), 29-29.

658 Xu, H., Shi, X., Ma, H., Lv, Y., Zhang, L., Mao, Z., 2011. The preparation and  
659 antibacterial effects of dopa-cotton/AgNPs. *Appl. Surf. Sci.* 257(15), 6799-6803.

660 Yu, S.J., Yin, Y.G., Chao, J.B., Shen, M.H., Liu, J.F., 2014. Highly dynamic PVP-coated  
661 silver nanoparticles in aquatic environments: chemical and morphology change induced  
662 by oxidation of Ag(0) and reduction of Ag(+). *Environ. Sci. Technol.* 48(1), 403-411.

663 Zhu, X., Zhou, L., Li, Y., Han, B., Feng, Q., 2021. Rapid Degradation of Carbon  
664 Tetrachloride by Microscale Ag/Fe Bimetallic Particles. *Int. J. Env. Res. Public Health*  
665 18(4), 2124.

666 Zhuang, Y., Ahn, S., Seyfferth, A.L., Masue-Slowey, Y., Fendorf, S., Luthy, R.G., 2011.  
667 Dehalogenation of polybrominated diphenyl ethers and polychlorinated biphenyl by  
668 bimetallic, impregnated, and nanoscale zerovalent iron. *Environ. Sci. Technol.* 45(11),  
669 4896-4903.

670